

Negative-temperature quantum magnetism in open dissipative systems

Masaya Nakagawa,^{1,*} Naoto Tsuji,² Norio Kawakami,³ and Masahito Ueda^{1,2}

¹*Department of Physics, University of Tokyo, 7-3-1 Hongo, Bunkyo-ku, Tokyo 113-0033, Japan*

²*RIKEN Center for Emergent Matter Science (CEMS), Wako, Saitama 351-0198, Japan*

³*Department of Physics, Kyoto University, Kyoto 606-8502, Japan*

(Dated: April 2, 2019)

In quantum magnetism, virtual particle exchange mediates an interaction between individual spins. Here we show that an inelastic Hubbard interaction, which leads to a loss of particles, dramatically alters spin-exchange processes and drives a system into spin states characterized by a negative absolute temperature. This mechanism is applicable to both fermionic and bosonic Mott insulators in any lattice geometry, and can naturally be realized with ultracold atoms undergoing two-body inelastic collisions. Negative-temperature spin correlations can be detected by using a double-well optical lattice or quantum-gas microscopy, the latter of which also serves to eliminate the effect of unwanted holes created by particle loss. Our results open a new avenue toward controlling quantum many-body states and heralds a novel approach to quantum simulations of magnetism.

Quantum magnetism in Mott insulators is one of the central problems in strongly correlated many-body systems [1]. A Mott insulator is described by the Hubbard model, where a strong repulsive interaction between particles precludes multiple occupation and anchors a single spin to each lattice site. While the kinetic motion of particles is frozen in Mott insulators, quantum mechanics allows particles to virtually hop between sites. A second-order process involving virtual exchange of particles leads to an effective spin-spin interaction, providing a fundamental origin of quantum magnetism [1]. Recent developments in quantum simulations of the Hubbard model with ultracold atoms [2] have offered a powerful approach to unveiling low-temperature properties of quantum magnets [3–7]. In particular, quantum-gas microscopy has enabled site-resolved imaging of spin states [8–11], culminating in direct observation of antiferromagnetic correlations and long-range order in the Hubbard model [12–15]. However, to observe quantum magnetism, it is necessary to achieve sufficiently low temperatures comparable with the exchange coupling. Currently, the difficulty of cooling atoms prevents observations of exotic quantum states of matter, such as topological order and quantum spin liquids, which have potential applications to topological quantum computation [16].

Here we demonstrate that ultracold atoms undergoing inelastic collisions obey a completely different principle for realizing quantum magnetism; instead of cooling down to low-energy states, those atoms realize a *negative-temperature* state (NTS) due to dissipation caused by inelastic collisions. Inelastic collisions have widely been observed for atoms in excited states [17, 18] and molecules [19, 20], and can be artificially induced by photoassociation [21]. In contrast to standard equilibrium systems which favor low-energy states, the long-time behavior of dissipative systems is governed by the imaginary part of energy, which characterizes the decay rate of each state. We show that the spin-exchange mechanism is dramatically altered in the presence of inelastic collisions due

to dissipation in an intermediate state, thereby realizing negative-temperature magnetism.

Our results are schematically summarized in Fig. 1. We consider a finite-size spin system which has an upper bound in the energy spectrum. Since the temperature T is defined in terms of energy E and entropy S as $1/T = \partial S/\partial E$, a NTS is realized when entropy has a negative slope against energy (see Fig. 1b) [22, 23]. We start from an equilibrium state at a positive temperature, which has an antiferromagnetic correlation in the case of the Fermi-Hubbard model (Fig. 1c). In a second-order process which mediates an interaction between spins, an antiferromagnetic spin configuration has a finite lifetime due to a loss in an intermediate state, whereas a ferromagnetic spin configuration cannot decay due to the Pauli exclusion principle (Fig. 1a). Because of this dissipative spin-exchange interaction, low-energy states gradually decay in the time evolution and the energy per particle monotonically increases. When the entropy is maximized, the system becomes an infinite-temperature state with vanishing spin correlation (Fig. 1d). Past that point, the population of higher-energy states surpasses that of lower-energy states, leading to the NTS characterized by a ferromagnetic spin correlation (Fig. 1e). Consequently, the magnetism is inverted. We note that, while NTSs have been realized in isolated systems [24–32], our system is essentially *open*; here, dissipation to an environment plays a vital role in the realization of a NTS.

Model.— We consider a dissipative Hubbard model of two-component fermions or bosons realized with ultracold atoms in an optical lattice. The unitary part of the dynamics is governed by the Hubbard Hamiltonian which reads

$$H = -t \sum_{\langle i,j \rangle, \sigma=\uparrow, \downarrow} (c_{i\sigma}^\dagger c_{j\sigma} + \text{h.c.}) + U \sum_j n_{j\uparrow}^{(f)} n_{j\downarrow}^{(f)} \quad (1)$$

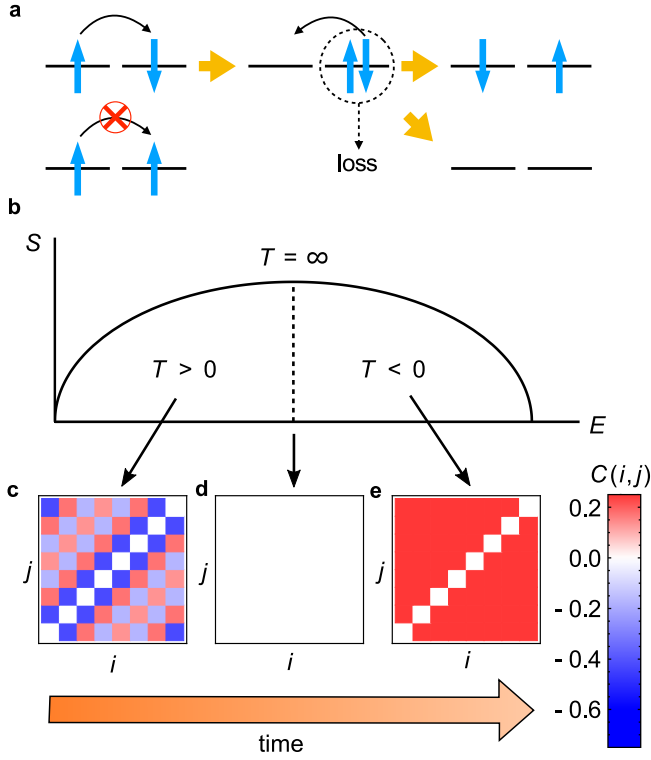


FIG. 1. **Schematic illustration of quantum magnetism in dissipative systems.** **a**, Spin-exchange interaction mediated by a second-order process. **b**, Entropy S as a function of energy E . **c-e**, Spin correlation $C(i, j) = \langle \psi | \mathbf{S}_i \cdot \mathbf{S}_j | \psi \rangle / \langle \psi | \psi \rangle$ ($i \neq j$) of the one-dimensional Fermi-Hubbard model with 8 sites. Through heating dynamics of the dissipative Hubbard model, an initial antiferromagnetic correlation at a positive temperature (c) is completely washed out at infinite temperature (d) and eventually a ferromagnetic correlation emerges at a negative temperature (e).

for fermions, and

$$H = -t \sum_{\langle i, j \rangle, \sigma = \uparrow, \downarrow} (b_{i\sigma}^\dagger b_{j\sigma} + \text{h.c.}) + \sum_j U_{\uparrow\downarrow} n_{j\uparrow}^{(b)} n_{j\downarrow}^{(b)} + \sum_\sigma \sum_j \frac{U_{\sigma\sigma}}{2} n_{j\sigma}^{(b)} (n_{j\sigma}^{(b)} - 1) \quad (2)$$

for bosons. Here $c_{j\sigma}$ ($b_{j\sigma}$) is the annihilation operator of a fermion (boson) with spin σ at site j , and $n_{j\sigma}^{(f)} = c_{j\sigma}^\dagger c_{j\sigma}$ ($n_{j\sigma}^{(b)} = b_{j\sigma}^\dagger b_{j\sigma}$). We assume that hopping occurs between nearest-neighbor sites and that the on-site elastic interactions are repulsive: $U, U_{\sigma\sigma'} > 0$. We assume $t > 0$ without loss of generality. Now we suppose that atoms also undergo inelastic collisions; because a large internal energy is converted to the kinetic energy, two atoms after inelastic collisions quickly escape from the trap and are lost. The dissipative dynamics of the density matrix ρ of the system is described by the following quantum master

equation [33]:

$$\frac{d\rho}{d\tau} = i[\rho, H] + \sum_{j, \sigma, \sigma'} \left(L_{j\sigma\sigma'} \rho L_{j\sigma\sigma'}^\dagger - \frac{1}{2} \{ L_{j\sigma\sigma'}^\dagger L_{j\sigma\sigma'}, \rho \} \right). \quad (3)$$

The Lindblad operators $L_{j\sigma\sigma'}$ induce two-body losses due to the on-site inelastic collisions, and are expressed as $L_{j\sigma\sigma'} = \sqrt{2\gamma} c_{j\sigma} c_{j\sigma'} \delta_{\sigma, \uparrow} \delta_{\sigma', \downarrow}$ for fermions and $L_{j\sigma\sigma'} = \sqrt{\gamma_{\sigma\sigma'}} b_{j\sigma} b_{j\sigma'}$ for bosons. The coefficients $\gamma, \gamma_{\sigma\sigma'} > 0$ are determined from the loss rates of atoms.

Spin-exchange interaction in the dissipative systems.— We first illustrate the basic mechanism that underlies the magnetism of the dissipative Hubbard system. We consider a strongly correlated regime ($U, U_{\sigma\sigma'} \gg t$) and assume that the initial particle density is set to unity so that a Mott insulating state is realized. For simplicity, we assume the spin SU(2) invariance, i.e., $U_{\uparrow\uparrow} = U_{\downarrow\downarrow} = U_{\uparrow\downarrow} = U$. Then, if double occupancies and holes are neglected, the Fermi (Bose) Hubbard model (1) ((2)) is well approximated by the antiferromagnetic (ferromagnetic) Heisenberg model $H_{\text{spin}} = J \sum_{\langle i, j \rangle} (\mathbf{S}_i \cdot \mathbf{S}_j - 1/4)$ ($H_{\text{spin}} = -J \sum_{\langle i, j \rangle} (\mathbf{S}_i \cdot \mathbf{S}_j + 3/4)$) with the spin-exchange interaction $J = 4t^2/U$ [34, 35].

Here we employ a quantum-trajectory method [36–38] to investigate the dynamics described by Eq. (3). The dynamics is decomposed into a non-unitary Schrödinger evolution under an effective non-Hermitian Hamiltonian $H_{\text{eff}} \equiv H - \frac{i}{2} \sum_\alpha L_\alpha^\dagger L_\alpha$ and stochastic quantum-jump processes which induce particle losses with the jump operators L_α . The non-Hermitian Hamiltonian H_{eff} is obtained by replacing the Hubbard interactions U and $U_{\sigma\sigma'}$ with $U - i\gamma$ and $U_{\sigma\sigma'} - i\gamma_{\sigma\sigma'}$, respectively, making the interaction coefficients complex-valued due to the inelastic interactions. In each quantum trajectory, the system evolves under the non-Hermitian Hubbard model during the time between loss events. Physically, the quantum trajectories are realized when the particle number of the system is continuously monitored [38–40]. This can be achieved in cold-atom experiments by using quantum-gas microscopy [12–15]. Each quantum trajectory is characterized by the number of loss events. As the simplest case, let us select a trajectory that does not contain any loss event; in this trajectory, the particle number is conserved to be the same as that of the initial state. Since the double occupancy is still suppressed due to the large Hubbard interaction U , the dynamics is constrained to the Hilbert subspace of the spin Hamiltonian. The effective spin Hamiltonian, which governs the dynamics in the quantum trajectory, is derived by the second-order perturbation theory from the non-Hermitian Hubbard model, giving

$$H_{\text{eff}} = \eta (J_{\text{eff}} + i\Gamma) \sum_{\langle i, j \rangle} \left(\mathbf{S}_i \cdot \mathbf{S}_j + \frac{1 - 2\eta}{4} \right) \quad (4)$$

with $J_{\text{eff}} = 4Ut^2/(U^2 + \gamma^2)$, $\Gamma = 4\gamma t^2/(U^2 + \gamma^2)$, and $\eta =$

+1 ($\eta = -1$) for fermions (bosons). Here we assume spin-independent dissipation $\gamma_{\sigma\sigma'} = \gamma$ for bosonic atoms. For a general case, see Supplementary Information. Equation (4) shows a remarkable feature; even if the system is restricted to the states without double occupancy, the spin-spin interactions are affected by dissipation since the virtual second-order process involves a doubly occupied site (see Fig. 1a). In fact, the energy denominators in $J_{\text{eff}} = \text{Re} \left[\frac{4t^2}{U-i\gamma} \right]$ and $\Gamma = \text{Im} \left[\frac{4t^2}{U-i\gamma} \right]$ clearly reflect the dissipation in the intermediate state. The eigenenergy of the Hamiltonian (4) is given by $E_n = (J_{\text{eff}} + i\Gamma)E_n^{(0)}/J$, where $E_n^{(0)} \leq 0$ is the eigenenergy of the Heisenberg model H_{spin} . Thus, the decay rate of the n -th eigenstate, which is given by the imaginary part of the energy, is proportional to $E_n^{(0)}$: $-\text{Im}[E_n] = -(\Gamma/J)E_n^{(0)} \geq 0$. Since $E_n^{(0)} \leq 0$, this indicates that lower-energy states have larger decay rates and thus have shorter lifetimes. Therefore, after a sufficiently long time, only the high-energy spin states can survive.

To be specific, we consider a situation in which the dissipative dynamics starts from an equilibrium initial state given by a Gibbs density matrix $\rho = e^{-\beta_i H_{\text{spin}}}/\text{Tr}[e^{-\beta_i H_{\text{spin}}}]$. At time $\tau = 0$, we switch on the dissipation; this situation corresponds to transferring atoms from the ground state to an excited state [17, 18] or applying a photoassociation laser [21] at $\tau = 0$. The time evolution of the density matrix under the lossless condition is given by

$$\begin{aligned} \rho(\tau) &= e^{-iH_{\text{eff}}\tau} \rho e^{iH_{\text{eff}}^\dagger\tau} \\ &\propto \sum_n e^{-\beta_i E_n^{(0)}} e^{2\text{Im}[E_n]\tau} |n\rangle \langle n| \\ &= \sum_n e^{-\beta(\tau) E_n^{(0)}} |n\rangle \langle n|, \end{aligned} \quad (5)$$

where $|n\rangle$ is the n -th eigenstate of H_{spin} , and $\beta(\tau) = \beta_i - 2(\Gamma/J)\tau$. Therefore, the spin system starting from a positive temperature $1/\beta_i > 0$ firstly becomes an infinite-temperature state at time $\tau = \tau_{\text{NT}} \equiv \beta_i J/(2\Gamma)$, and then evolves into a NTS with $1/\beta(\tau > \tau_{\text{NT}}) < 0$ (see Fig. 1c-e). We note that the NTS can be regarded as a positive-temperature state of a Hamiltonian $-H_{\text{spin}}$. Thus, in the NTS, the antiferromagnetic (ferromagnetic) Heisenberg model exhibits a ferromagnetic (antiferromagnetic) correlation, as shown in Fig. 1e. The time scale of this ‘‘heating’’ dynamics is characterized by the imaginary part of the exchange interaction Γ , which takes the maximum value $\Gamma = 0.5J$ at $\gamma = U$ as a function of γ .

Double-well systems.— A minimal setup to demonstrate the basic principle shown above is a two-site system. It can be experimentally realized with an ensemble of double wells created by optical superlattices [3, 4], and magnetic correlations between the left and right wells can be measured from singlet-triplet oscillations [4, 5, 7]. We consider an ensemble of double wells in which two parti-

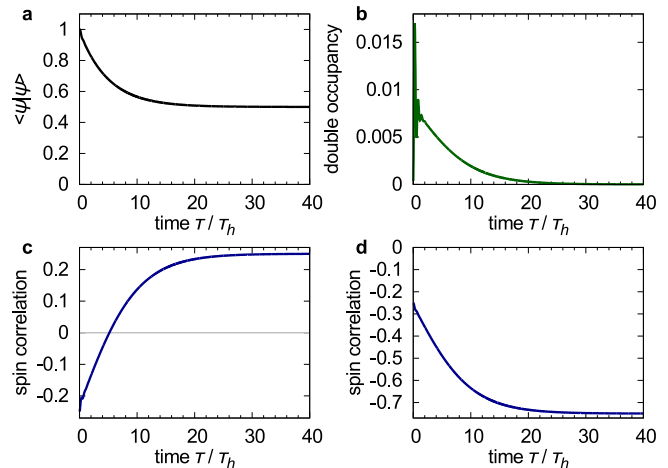


FIG. 2. **Dynamics of dissipative Hubbard models in two-site systems.** **a, b**, Time evolution of the squared norm $\langle \psi(\tau) | \psi(\tau) \rangle$ (**a**) and double occupancy $\langle \psi(\tau) | \frac{1}{2}(n_{1\uparrow}^{(a)} n_{1\downarrow}^{(a)} + n_{2\uparrow}^{(a)} n_{2\downarrow}^{(a)}) | \psi(\tau) \rangle / \langle \psi(\tau) | \psi(\tau) \rangle$ ($a = f$ or b) (**b**), both of which take the same values for the Fermi and Bose Hubbard models. **c, d**, Time evolution of the spin correlation $\langle \psi(\tau) | \mathbf{S}_1 \cdot \mathbf{S}_2 | \psi(\tau) \rangle / \langle \psi(\tau) | \psi(\tau) \rangle$ of the Fermi (**c**) and Bose (**d**) Hubbard models. The parameters are set to $U/t = 10$ and $\gamma/t = 3$. The unit of time is the inverse of the hopping rate $\tau_h = 1/t$.

cles with opposite spins occupy each double well. During the dissipative dynamics, a double well in which a loss event takes place becomes empty. Therefore, when a magnetic correlation is measured at time τ , signals come from double wells where particles are still not lost. Such wells are faithfully described by the quantum trajectory method without loss events.

Figure 2 shows the time evolution of the squared norm of the state $\langle \psi(\tau) | \psi(\tau) \rangle$, double occupancy $\langle \psi(\tau) | \frac{1}{2}(n_{1\uparrow}^{(a)} n_{1\downarrow}^{(a)} + n_{2\uparrow}^{(a)} n_{2\downarrow}^{(a)}) | \psi(\tau) \rangle / \langle \psi(\tau) | \psi(\tau) \rangle$ ($a = f, b$), and spin correlation $\langle \psi(\tau) | \mathbf{S}_1 \cdot \mathbf{S}_2 | \psi(\tau) \rangle / \langle \psi(\tau) | \psi(\tau) \rangle$ obtained from a numerical solution of the Schrödinger equation $i\partial_\tau |\psi(\tau)\rangle = H_{\text{eff}} |\psi(\tau)\rangle$. Here H_{eff} is the two-site non-Hermitian Fermi (Bose) Hubbard model and the initial state is assumed to be $c_{1\uparrow}^\dagger c_{2\downarrow}^\dagger |0\rangle$ ($b_{1\uparrow}^\dagger b_{2\downarrow}^\dagger |0\rangle$), where $|0\rangle$ is a vacuum. The results clearly show that the dissipative Fermi (Bose) Hubbard system develops a ferromagnetic (antiferromagnetic) correlation which is finally saturated at 0.25 (-0.75), indicating a formation of the highest-energy spin state $(|\uparrow\rangle_1 |\downarrow\rangle_2 + |\downarrow\rangle_1 |\uparrow\rangle_2)/\sqrt{2}$ ($(|\uparrow\rangle_1 |\downarrow\rangle_2 - |\downarrow\rangle_1 |\uparrow\rangle_2)/\sqrt{2}$) of the Heisenberg model. We note that the double occupancy in the dynamics is almost negligible and further suppressed by an increase in the dissipation γ (see Supplementary Information for the dependence on γ); the latter is due to the continuous quantum Zeno effect [19–21] by which strong dissipation inhibits hopping to an occupied site. Nevertheless, the virtual hopping process is allowed, leading to the growth of spin

correlation.

Another important feature is that the squared norm stays constant after the spin correlation is saturated. Since the squared norm corresponds to the probability of the lossless quantum trajectory [38], it means that the system enters a dark state which is immune to the dissipation. This property explains why the highest-energy spin state is realized in the long-time limit; the spin-symmetric (spin-antisymmetric) state of fermions (bosons) is actually free from dissipation and thus has the longest lifetime, since in this spin configuration both Fermi and Bose statistics dictate antisymmetry of the real-space wavefunction and hence allows no double occupancy [41].

Eliminating holes with conditional correlators.— Having established the basic mechanism of the negative-temperature quantum magnetism, we address an important question for experimental realizations; how is a NTS affected by holes created by particle loss? The holes propagate in the system, scramble the background spin configuration, and disturb the development of spin correlations. Below we show that this difficulty is circumvented by using quantum-gas microscopy for the one-dimensional Hubbard model. This experimental technique enables a high-precision measurement of the particle number at the single-site level [8–11]. Given a single-shot image of an atomic gas, the occupation number of each site is identified to be zero, one, two, etc. To extract spin correlations between sites occupied by a single spin, we define a conditional correlator

$$C_{\text{proj}}(j, j+1) \equiv \frac{\langle \psi(\tau) | P_j P_{j+1} \mathbf{S}_j \cdot \mathbf{S}_{j+1} P_j P_{j+1} | \psi(\tau) \rangle}{\langle \psi(\tau) | P_j P_{j+1} | \psi(\tau) \rangle}. \quad (6)$$

Here P_j is a projector onto those states in which site j is singly occupied. More generally, we can use a correlation function $C_{\text{proj}}(j, j+d; d_h) \equiv \langle \psi(\tau) | P_j Q_{d_h} P_{j+d} \mathbf{S}_j \cdot \mathbf{S}_{j+d} P_j Q_{d_h} P_{j+d} | \psi(\tau) \rangle / \langle \psi(\tau) | P_j Q_{d_h} P_{j+d} | \psi(\tau) \rangle$, where Q_{d_h} is another projector onto states with d_h holes and $d - d_h - 1$ singly occupied sites between sites j and $j+d$. Such conditional correlators have been measured in experiments with quantum-gas microscopy [42, 43] by collecting images that match the conditions.

We first show in Fig. 3 the time evolution of the one-dimensional dissipative Hubbard models in quantum trajectories without loss events. The system size is $N = 8$ ($N = 6$) for the Fermi (Bose) system (see Methods). The initial states are chosen to be a Néel state $|\uparrow\downarrow\uparrow\downarrow\uparrow\downarrow\rangle$ and a ferromagnetic domain-wall state $|\uparrow\uparrow\downarrow\downarrow\rangle$ for the Fermi and Bose systems, respectively. The dissipative Fermi (Bose) system in Fig. 3b (3d) clearly develops a ferromagnetic (antiferromagnetic) spin correlation $C(i, j) = \langle \psi(\tau) | \mathbf{S}_i \cdot \mathbf{S}_j | \psi(\tau) \rangle / \langle \psi(\tau) | \psi(\tau) \rangle$ which is inverted from that of the initial state, and it is saturated at a value consistent with the ground state of the ferromagnetic (antiferromagnetic) Heisenberg chain.

However, as seen from Figs. 3a and 3c, the fast decay of the squared norm indicates that the probability of the lossless trajectory becomes small after a long time, and thus a loss event inevitably takes place [44].

Figure 4a (4c) shows dynamics of the conditional correlators of the dissipative Fermi (Bose) Hubbard model calculated from a single quantum trajectory which contains a loss event. Additional numerical data are available in Supplementary Information. The initial state is the same as in Fig. 3. In Fig. 4a (4c), a quantum-jump event takes place at $\tau/\tau_h \simeq 3$ ($\tau/\tau_h \simeq 1.7$) and creates a hole at site $j = 0$. Remarkably, although the ferromagnetic (antiferromagnetic) correlation, which develops through the dissipative exchange mechanism, is disturbed once by a quantum jump, it starts to grow again and is finally saturated at the value same as in the case of no quantum jump.

Notably, such a development of the spin correlation cannot clearly be detected by using a standard spin correlator $C(i, j)$ (Figs. 4b and 4d), since the motion of a hole disturbs the spin configuration. In this sense, the ferromagnetic/antiferromagnetic correlations are reminiscent of the hidden correlation in hole-doped Mott insulators [43], which is a hallmark of spin-charge separation in the one-dimensional systems [45]. In the strongly correlated Hubbard chain, the created holes move freely as if they were non-interacting, while the background spin state remains the same as that of the Heisenberg chain [46]. In particular, given an eigenstate of the one-dimensional Hubbard chain, one can reconstruct an eigenstate of the Heisenberg model by eliminating holes contained in each particle configuration superposed in the quantum state [43, 46, 47]. Thus, the conditional correlators $C_{\text{proj}}(j, j+1)$ and $C_{\text{proj}}(j, j+d; d_h)$ capture the spin correlations in the background Heisenberg model, and are equivalent to $\langle \mathbf{S}_j \cdot \mathbf{S}_{j+1} \rangle_{\text{H}}$ and $\langle \mathbf{S}_j \cdot \mathbf{S}_{j+d-d_h} \rangle_{\text{H}}$, respectively (here $\langle \rangle_{\text{H}}$ denotes the expectation value taken for the Heisenberg model). This explains the saturated value of the conditional spin correlation that exactly coincides with that in the trajectory without loss events shown in Fig. 3b. Although the original argument on the hidden correlation was limited to the Fermi-Hubbard model [43, 46, 47], our numerical results indicate that this mechanism also works for the bosonic Hubbard system.

Summary and future perspectives.— In summary, we have shown that the inelastic Hubbard interaction alters the spin-exchange process due to a finite lifetime of the intermediate state, leading to novel quantum magnetism opposite to the standard equilibrium magnetism; rather than stabilizing low-energy states, high-energy spin states have longer lifetimes and are thus realized in the dissipative systems. The Hubbard model with inelastic interactions can be realized with various types of ultracold atoms in internal excited states; for example, ytterbium atoms are a promising candidate for implementation for their long-lived excited states for which the decay

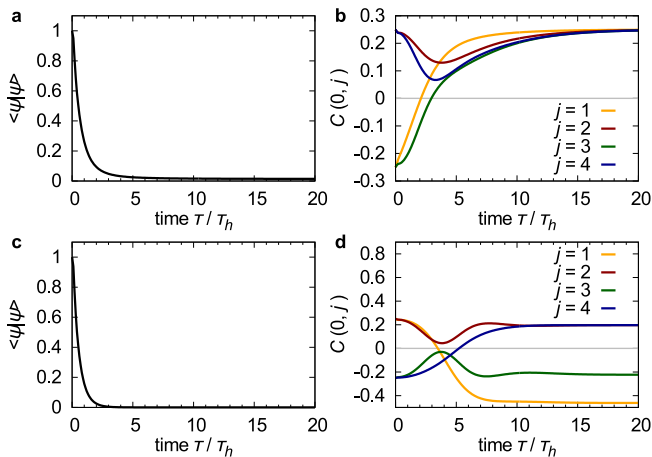


FIG. 3. **Dynamics of one-dimensional dissipative Hubbard models without loss events.** Time evolution of the squared norm $\langle \psi(\tau) | \psi(\tau) \rangle$ (a and c) and spin correlation $C(0, j)$ (b and d) for the Fermi (a and b) and Bose (c and d) Hubbard systems. The parameters are set to $U/t = 10$ and $\gamma/t = 10$. The unit of time is the inverse of the hopping rate $\tau_h = 1/t$.

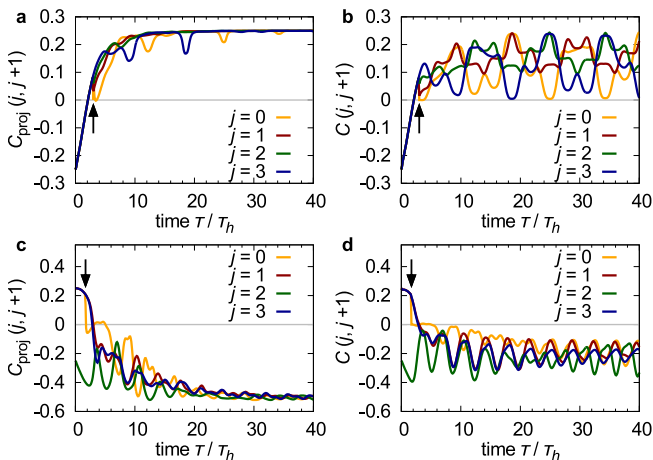


FIG. 4. **Conditional spin correlation vs. standard spin correlation.** Dynamics of conditional spin correlation $C_{\text{proj}}(j, j+1)$ (a and c) and standard spin correlation $C(j, j+1)$ (b and d) in a quantum trajectory of the dissipative Fermi (a and b) and Bose (c and d) Hubbard model with a loss event. The parameters are the same as in Fig. 3. The arrows indicate the time at which the loss event takes place. The unit of time is the inverse of the hopping rate $\tau_h = 1/t$.

to the ground state due to spontaneous emission is negligible [17, 18]. Furthermore, inelastic collisions can be artificially induced by using photoassociation techniques [21], which will enable the control of quantum magnetism with a NTS.

Our work raises many open questions for future investigation. First, while we have shown that the effect of holes can be eliminated in one-dimensional systems, the interplay between holes and background spin config-

urations is more intricate in two (or higher) dimensions. Second, since the bosonic Hubbard system develops antiferromagnetic correlations in a NTS, geometric frustration in the lattice may realize quantum spin liquids and topological order, which have not yet been realized in cold-atom experiments due to the difficulty of cooling. Third, in this paper, we have focused on the cases with spin $SU(2)$ symmetry. If this symmetry is relaxed, eigenstates of the non-Hermitian spin Hamiltonian with the complex-valued spin-exchange interaction are no longer the same as those of the original Hermitian spin Hamiltonian. Thus, in these systems, novel quantum magnetism with non-Hermitian spin Hamiltonians [48] may be realized.

Acknowledgments

We thank Kazuya Fujimoto, Takeshi Fukuhara, and Yoshiro Takahashi for helpful discussions. This work was supported by KAKENHI (Grants No. JP16K05501, No. JP16K17729, No. JP18H01140, and No. JP18H01145) and a Grant-in-Aid for Scientific Research on Innovative Areas (KAKENHI Grant No. JP15H05855) from the Japan Society for the Promotion of Science. M.N. was supported by RIKEN Special Postdoctoral Researcher Program.

Author contributions

M.N. conceived the main idea. M.N. and N.T. performed the numerical simulations. All authors contributed to analyzing and interpreting the results.

Competing interests

The authors declare no competing interests.

Methods

Numerical simulations.— The dynamics of the dissipative Hubbard model is simulated by using a quantum trajectory method [36–38]. According to a random number R_1 taken from an interval $0 \leq R_1 \leq 1$, the system evolves under the nonunitary Schrödinger equation $i\partial_\tau |\psi(\tau)\rangle = H_{\text{eff}} |\psi(\tau)\rangle$ up to a time τ_1 when the squared norm $\langle \psi(\tau_1) | \psi(\tau_1) \rangle$ is equal to R_1 . Here H_{eff} is the N -site non-Hermitian Fermi or Bose Hubbard model under the periodic boundary condition. The Schrödinger dynamics is numerically calculated by using exact diagonalization of H_{eff} . At time τ_1 , the loss event takes place and the state is multiplied by a quantum-jump operator $L_{j\sigma\sigma'}$ and then normalized:

$$|\psi(\tau_1 + 0)\rangle = \frac{L_{j\sigma\sigma'} |\psi(\tau_1 - 0)\rangle}{\sqrt{\langle \psi(\tau_1 - 0) | L_{j\sigma\sigma'}^\dagger L_{j\sigma\sigma'} | \psi(\tau_1 - 0) \rangle}}. \quad (7)$$

The Lindblad operator $L_{j\sigma\sigma'}$ for the loss event at time

τ_1 is selected according to the probability

$$\frac{\langle \psi(\tau_1 - 0) | L_{j\sigma\sigma'}^\dagger L_{j\sigma\sigma'} | \psi(\tau_1 - 0) \rangle}{\sum_{j,\sigma,\sigma'} \langle \psi(\tau_1 - 0) | L_{j\sigma\sigma'}^\dagger L_{j\sigma\sigma'} | \psi(\tau_1 - 0) \rangle}. \quad (8)$$

After the time τ_1 , we take another random number R_2 and repeat the above procedure.

* nakagawa@cat.phys.s.u-tokyo.ac.jp

- [1] Auerbach, A. *Interacting Electrons and Quantum Magnetism*. (Springer-Verlag, New York, 1994).
- [2] Esslinger, T. Fermi-Hubbard Physics with Atoms in an Optical Lattice. *Annu. Rev. Condens. Matter Phys.* **1**, 129–152 (2010).
- [3] Trotzky, S. *et al.* Time-Resolved Observation and Control of Superexchange Interactions with Ultracold Atoms in Optical Lattices. *Science* **319**, 295–299 (2008).
- [4] Greif, D., Uehlinger, T., Jotzu, G., Tarruell, L. & Esslinger, T. Short-Range Quantum Magnetism of Ultracold Fermions in an Optical Lattice. *Science* **340**, 1307–1310 (2013).
- [5] Greif, D., Jotzu, G., Messer, M., Desbuquois, R. & Esslinger, T. Formation and Dynamics of Antiferromagnetic Correlations in Tunable Optical Lattices. *Phys. Rev. Lett.* **115**, 260401 (2015).
- [6] Hart, R. A. *et al.* Observation of antiferromagnetic correlations in the Hubbard model with ultracold atoms. *Nature* **519**, 211–214 (2015).
- [7] Ozawa, H., Taie, S., Takasu, Y., & Takahashi, Y. Antiferromagnetic Spin Correlation of $SU(N)$ Fermi Gas in an Optical Superlattice. *Phys. Rev. Lett.* **121**, 225303 (2018).
- [8] Bakr, W. S., Gillen, J. I., Peng, A., Fölling, S., & Greiner, M. A quantum gas microscope for detecting single atoms in a Hubbard-regime optical lattice. *Nature* **462**, 74–77 (2009).
- [9] Parsons, M. F. *et al.* Site-Resolved Imaging of Fermionic ^6Li in an Optical Lattice. *Phys. Rev. Lett.* **114**, 213002 (2015).
- [10] Cheuk, L. *et al.* Quantum-Gas Microscope for Fermionic Atoms. *Phys. Rev. Lett.* **114**, 193001 (2015).
- [11] Cheuk, L. *et al.* Observation of 2D Fermionic Mott Insulators of ^{40}K with Single-Site Resolution. *Phys. Rev. Lett.* **116**, 235301 (2016).
- [12] Parsons, M. F. *et al.* Site-resolved measurement of the spin-correlation function in the Fermi-Hubbard model. *Science* **353**, 1253–1256 (2016).
- [13] Cheuk, L. *et al.* Observation of spatial charge and spin correlations in the 2D Fermi-Hubbard model. *Science* **353**, 1260–1264 (2016).
- [14] Boll, M. *et al.* Spin- and density-resolved microscopy of antiferromagnetic correlations in Fermi-Hubbard chains. *Science* **353**, 1257–1260 (2016).
- [15] Mazurenko, A. *et al.* A cold-atom Fermi-Hubbard antiferromagnet. *Nature* **545**, 462–466 (2017).
- [16] Kitaev, A. Anyons in an exactly solved model and beyond. *Ann. Phys.* **321**, 2–111 (2006).
- [17] Sponselee, K. *et al.* Dynamics of ultracold quantum gases in the dissipative Fermi-Hubbard model. *Quantum Sci. Technol.* **4**, 014002 (2018).
- [18] Tomita, T., Nakajima, S., Takasu, Y., & Takahashi, Y. Dissipative Bose-Hubbard system with intrinsic two-body loss. *Phys. Rev. A* **99**, 031601 (2019).
- [19] Syassen, N. *et al.* Strong Dissipation Inhibits Losses and Induces Correlations in Cold Molecular Gases. *Science* **320**, 1329–1331 (2008).
- [20] Zhu, B. *et al.* Suppressing the Loss of Ultracold Molecules Via the Continuous Quantum Zeno Effect. *Phys. Rev. Lett.* **112**, 070404 (2014).
- [21] Tomita, T., Nakajima, S., Danshita, I., Takasu, Y., & Takahashi, Y. Observation of the Mott insulator to superfluid crossover of a driven-dissipative Bose-Hubbard system. *Sci. Adv.* **3**, e1701513 (2017).
- [22] Landau, L. D. & Lifshitz, E. M. *Statistical Physics Part 1*. (Butterworth-Heinemann, Oxford, 1984).
- [23] Ramsey, N. F. Thermodynamics and Statistical Mechanics at Negative Absolute Temperatures. *Phys. Rev.* **103**, 20–28 (1956).
- [24] Purcell, E. M. & Pound, R. V. A Nuclear Spin System at Negative Temperature. *Phys. Rev.* **81**, 279–280 (1951).
- [25] Hakonen, P. J., Nummila, K. K., Vuorinen, R. T. & Lounasmaa, O. V. Observation of nuclear ferromagnetic ordering in silver at negative nanokelvin temperatures. *Phys. Rev. Lett.* **68**, 365–368 (1992).
- [26] Hakonen, P. & Lounasmaa, O. V. Negative Absolute Temperatures: "Hot" Spins in Spontaneous Magnetic Order. *Science* **265**, 1821–1825 (1994).
- [27] Rapp, A., Mandt, S. & Rosch, A. Equilibration Rates and Negative Absolute Temperatures for Ultracold Atoms in Optical Lattices. *Phys. Rev. Lett.* **105**, 220405 (2010).
- [28] Rapp, A. Quantum simulators at negative absolute temperatures. *Phys. Rev. A* **85**, 043612 (2012).
- [29] Tsuji, N., Oka, T., Werner, P. & Aoki, H. Dynamical Band Flipping in Fermionic Lattice Systems: An ac-Field-Driven Change of the Interaction from Repulsive to Attractive. *Phys. Rev. Lett.* **106**, 236401 (2011).
- [30] Braun, S. *et al.* Negative Absolute Temperature for Motional Degrees of Freedom. *Science* **339**, 52–55 (2013).
- [31] Gauthier, G. *et al.* Negative-Temperature Onsager Vortex Clusters in a Quantum Fluid. Preprint at <http://arxiv.org/abs/1801.06951> (2018).
- [32] Johnstone, S. P. *et al.* Order from chaos: Observation of large-scale flow from turbulence in a two-dimensional superfluid. Preprint at <http://arxiv.org/abs/1801.06952> (2018).
- [33] Breuer, H. P. & Petruccione, F. *The Theory of Open Quantum Systems*. (Oxford University Press, Oxford, 2007).
- [34] Kuklov, A. B. & Svistunov, B. V. Counterflow Superfluidity of Two-Species Ultracold Atoms in a Commensurate Optical Lattice. *Phys. Rev. Lett.* **90**, 100401 (2003).
- [35] Duan, L.-M., Demler, E. & Lukin, M. D. Controlling Spin Exchange Interactions of Ultracold Atoms in Optical Lattices. *Phys. Rev. Lett.* **91**, 090402 (2003).
- [36] Dalibard, J., Castin, Y. & Mølmer, K. Wave-function approach to dissipative processes in quantum optics. *Phys. Rev. Lett.* **68**, 580–583 (1992).
- [37] Carmichael, H. J. Quantum trajectory theory for cascaded open systems. *Phys. Rev. Lett.* **70**, 2273–2276 (1993).
- [38] Daley, A. J. Quantum trajectories and open many-body quantum systems. *Adv. Phys.* **63**, 77–149 (2014).
- [39] Ashida, Y., Furukawa, S. & Ueda, M. Quantum critical behavior influenced by measurement backaction in ultra-

- cold gases. *Phys. Rev. A* **94**, 053615 (2016).
- [40] Ashida, Y., Saito, K. & Ueda, M. Thermalization and Heating Dynamics in Open Generic Many-Body Systems. *Phys. Rev. Lett.* **121**, 170402 (2018).
- [41] Foss-Feig, M., Daley, A. J., Thompson, J. K. & Rey, A. M. Steady-State Many-Body Entanglement of Hot Reactive Fermions. *Phys. Rev. Lett.* **109**, 230501 (2012).
- [42] Endres, M. *et al.* Observation of Correlated Particle-Hole Pairs and String Order in Low-Dimensional Mott Insulators. *Science* **334**, 200–203 (2011).
- [43] Hilker, T. A. *et al.* Revealing hidden antiferromagnetic correlations in doped Hubbard chains via string correlators. *Science* **357**, 484–487 (2017).
- [44] In the N -particle Fermi-Hubbard system, the long-time limit of the squared norm approaches a squared overlap between the initial state and the dark state (the spin-symmetric Dicke state [41]) and is given by $[(N/2)!]^2/N!$. On the other hand, since N spins cannot form a perfect antisymmetric state, the Bose-Hubbard system does not have a dark state except for $N = 2$.
- [45] Giamarchi, T. *Quantum Physics in One Dimension*. (Oxford University Press, Oxford, 2003).
- [46] Ogata, M & Shiba, H. Bethe-ansatz wave function, momentum distribution, and spin correlation in the one-dimensional strongly correlated Hubbard model. *Phys. Rev. B* **41**, 2326–2338 (1990).
- [47] Kruis, H. V., McCulloch, I. P., Nussinov, Z. & Zaanen, J. Geometry and the hidden order of Luttinger liquids: The universality of squeezed space. *Phys. Rev. B* **70**, 075109 (2004).
- [48] Lee, T. E. & Chan, C.-K. Heralded Magnetism in Non-Hermitian Atomic Systems. *Phys. Rev. X* **4**, 041001 (2014).

Supplementary Information for
“Negative-temperature quantum magnetism in open dissipative systems”

Non-Hermitian spin Hamiltonian

We derive the non-Hermitian spin Hamiltonian which governs the time evolution in a strongly correlated regime. We start with an effective non-Hermitian Hubbard Hamiltonian H_{eff} and divide it into the kinetic part H' and the interaction part H_0 , where each part reads

$$H' = -t \sum_{\langle i,j \rangle} \sum_{\sigma=\uparrow,\downarrow} (c_{i\sigma}^\dagger c_{j\sigma} + \text{h.c.}),$$

$$H_0 = (U - i\gamma) \sum_j n_{j\uparrow}^{(f)} n_{j\downarrow}^{(f)},$$

for fermions, and

$$H' = -t \sum_{\langle i,j \rangle} \sum_{\sigma=\uparrow,\downarrow} (b_{i\sigma}^\dagger b_{j\sigma} + \text{h.c.}),$$

$$H_0 = (U_{\uparrow\downarrow} - i\gamma_{\uparrow\downarrow}) \sum_j n_{j\uparrow}^{(b)} n_{j\downarrow}^{(b)} + \sum_j \sum_{\sigma=\uparrow,\downarrow} \frac{U_{\sigma\sigma} - i\gamma_{\sigma\sigma}}{2} n_{j\sigma}^{(b)} (n_{j\sigma}^{(b)} - 1),$$

for bosons. In the strongly correlated regime $U, U_{\sigma\sigma'} \gg t$, the kinetic term H' can be treated as a perturbation. For simplicity, here we assume that a Mott insulating state is realized and neglect holes in the Mott insulator. According to the second-order perturbation theory, an effective Hamiltonian is given by

$$H_{\text{spin}} = E_0 + \mathcal{P} H' \frac{1}{E_0 - H_0} H' \mathcal{P}, \quad (\text{S1})$$

where \mathcal{P} is a projector onto the Hilbert subspace in which each lattice site is occupied by one atom. Here the energy E_0 of the unperturbed state is set to $E_0 = 0$. In the simplest two-site case, the Hilbert subspace is spanned by four spin configurations $\{|\uparrow\uparrow\rangle, |\uparrow\downarrow\rangle, |\downarrow\uparrow\rangle, |\downarrow\downarrow\rangle\}$. In this case, the spin Hamiltonian reads

$$H_{\text{spin}} = -\frac{2t^2}{U - i\gamma} (|\uparrow\downarrow\rangle \langle\uparrow\downarrow| + |\downarrow\uparrow\rangle \langle\downarrow\uparrow| - |\downarrow\uparrow\rangle \langle\uparrow\downarrow| - |\uparrow\downarrow\rangle \langle\downarrow\uparrow|) \quad (\text{S2})$$

for fermions, and

$$H_{\text{spin}} = -2t^2 \left(\frac{2}{U_{\uparrow\uparrow} - i\gamma_{\uparrow\uparrow}} |\uparrow\uparrow\rangle \langle\uparrow\uparrow| + \frac{2}{U_{\downarrow\downarrow} - i\gamma_{\downarrow\downarrow}} |\downarrow\downarrow\rangle \langle\downarrow\downarrow| + \frac{1}{U_{\uparrow\downarrow} - i\gamma_{\uparrow\downarrow}} |\uparrow\downarrow\rangle \langle\uparrow\downarrow| + \frac{1}{U_{\uparrow\downarrow} - i\gamma_{\uparrow\downarrow}} |\downarrow\uparrow\rangle \langle\downarrow\uparrow| \right. \\ \left. + \frac{1}{U_{\uparrow\downarrow} - i\gamma_{\uparrow\downarrow}} |\downarrow\uparrow\rangle \langle\uparrow\downarrow| + \frac{1}{U_{\uparrow\downarrow} - i\gamma_{\uparrow\downarrow}} |\uparrow\downarrow\rangle \langle\downarrow\uparrow| \right), \quad (\text{S3})$$

for bosons. Hence, for fermionic atoms, the spin Hamiltonian is given by the non-Hermitian Heisenberg model

$$H_{\text{spin}} = \frac{4t^2}{U - i\gamma} \sum_{\langle i,j \rangle} \left(\mathbf{S}_i \cdot \mathbf{S}_j - \frac{1}{4} \right), \quad (\text{S4})$$

and for bosonic atoms it is given by

$$H_{\text{spin}} = \sum_{\langle i,j \rangle} \left[-\frac{4t^2}{U_{\uparrow\downarrow} - i\gamma_{\uparrow\downarrow}} (S_i^x S_j^x + S_i^y S_j^y) - 4t^2 \left(\frac{1}{U_{\uparrow\uparrow} - i\gamma_{\uparrow\uparrow}} + \frac{1}{U_{\downarrow\downarrow} - i\gamma_{\downarrow\downarrow}} - \frac{1}{U_{\uparrow\downarrow} - i\gamma_{\uparrow\downarrow}} \right) S_i^z S_j^z \right. \\ \left. - t^2 \left(\frac{1}{U_{\uparrow\uparrow} - i\gamma_{\uparrow\uparrow}} + \frac{1}{U_{\downarrow\downarrow} - i\gamma_{\downarrow\downarrow}} + \frac{1}{U_{\uparrow\downarrow} - i\gamma_{\uparrow\downarrow}} \right) - 2t^2 \left(\frac{1}{U_{\uparrow\uparrow} - i\gamma_{\uparrow\uparrow}} - \frac{1}{U_{\downarrow\downarrow} - i\gamma_{\downarrow\downarrow}} \right) (S_i^z + S_j^z) \right] \\ = \sum_{\langle i,j \rangle} \left[(J_{\text{eff}}^\perp + i\Gamma^\perp) (S_i^x S_j^x + S_i^y S_j^y) + (J_{\text{eff}}^z + i\Gamma^z) S_i^z S_j^z + C \right] + (h_r + ih_i) \sum_j S_j^z, \quad (\text{S5})$$

where

$$J_{\text{eff}}^{\perp} = -\text{Re} \left[\frac{4t^2}{U_{\uparrow\downarrow} - i\gamma_{\uparrow\downarrow}} \right], \quad (\text{S6})$$

$$\Gamma^{\perp} = -\text{Im} \left[\frac{4t^2}{U_{\uparrow\downarrow} - i\gamma_{\uparrow\downarrow}} \right], \quad (\text{S7})$$

$$J_{\text{eff}}^z = -4t^2 \text{Re} \left[\frac{1}{U_{\uparrow\uparrow} - i\gamma_{\uparrow\uparrow}} + \frac{1}{U_{\downarrow\downarrow} - i\gamma_{\downarrow\downarrow}} - \frac{1}{U_{\uparrow\downarrow} - i\gamma_{\uparrow\downarrow}} \right], \quad (\text{S8})$$

$$\Gamma^z = -4t^2 \text{Im} \left[\frac{1}{U_{\uparrow\uparrow} - i\gamma_{\uparrow\uparrow}} + \frac{1}{U_{\downarrow\downarrow} - i\gamma_{\downarrow\downarrow}} - \frac{1}{U_{\uparrow\downarrow} - i\gamma_{\uparrow\downarrow}} \right], \quad (\text{S9})$$

$$C = -t^2 \left(\frac{1}{U_{\uparrow\uparrow} - i\gamma_{\uparrow\uparrow}} + \frac{1}{U_{\downarrow\downarrow} - i\gamma_{\downarrow\downarrow}} + \frac{1}{U_{\uparrow\downarrow} - i\gamma_{\uparrow\downarrow}} \right), \quad (\text{S10})$$

$$h_r = -2zt^2 \text{Re} \left[\frac{1}{U_{\uparrow\uparrow} - i\gamma_{\uparrow\uparrow}} - \frac{1}{U_{\downarrow\downarrow} - i\gamma_{\downarrow\downarrow}} \right], \quad (\text{S11})$$

$$h_i = -2zt^2 \text{Im} \left[\frac{1}{U_{\uparrow\uparrow} - i\gamma_{\uparrow\uparrow}} - \frac{1}{U_{\downarrow\downarrow} - i\gamma_{\downarrow\downarrow}} \right]. \quad (\text{S12})$$

Here, z denotes the coordination number of the lattice. By setting $U_{\uparrow\uparrow} = U_{\downarrow\downarrow} = U_{\uparrow\downarrow} = U$ and $\gamma_{\uparrow\uparrow} = \gamma_{\downarrow\downarrow} = \gamma_{\uparrow\downarrow} = \gamma$, the model for bosons (S5) is reduced to the non-Hermitian Heisenberg model considered in the main text. If a bosonic system does not respect the spin $SU(2)$ symmetry, the non-Hermitian spin model (S5) is an XXZ model with complex-valued spin-spin interactions and a magnetic field. We note that the effective magnetic field has an imaginary part h_i in general. In the Hermitian case, the real magnetic field h_r can be compensated by using an additional external magnetic field [35]. However, the imaginary magnetic field cannot be compensated by any real external field and thus inevitably affects the behavior of dissipative spin systems.

Dissipation dependence of the dynamics

In Fig. S1, we show how the real and imaginary parts of the effective spin-exchange interactions, which are respectively given by $J_{\text{eff}} = 4Ut^2/(U^2 + \gamma^2)$ and $\Gamma = 4\gamma t^2/(U^2 + \gamma^2)$, depend on the inelastic-collision rate γ . The imaginary part takes its maximum $\Gamma = 0.5J$ at $\gamma/U = 1$ and then decreases with the increase of γ . The suppression of the effective dissipation rate Γ at large γ is attributed to the continuous quantum Zeno effect [19–21], which freezes the hopping of atoms due to the large dissipation. On the other hand, the real part J_{eff} of the spin-exchange interaction monotonically decreases as a function of γ .

The dependence of the dynamics of the Hubbard model on dissipation is shown in Fig. S2. Here we calculate the dynamics of the two-site non-Hermitian Fermi and Bose Hubbard models which can be realized with a double-well optical lattice as mentioned in the main text. When small dissipation is introduced to the system (Figs. S2 **a-d**), fast oscillations of the double occupancy and the spin correlation due to the large on-site repulsion U are damped by the dissipation. As the strength of dissipation is increased (Figs. S2 **e-h**), the development of the ferromagnetic (antiferromagnetic) spin correlation in the Fermi (Bose) system is accelerated by an increase in the imaginary part of the spin-exchange interaction Γ , which governs the time scale of the dissipative spin dynamics. At the optimal value $\gamma/U = 1$ (Figs. S2 **i-l**), the fastest development of the spin correlation is observed. We note that the double occupancy is gradually suppressed with increasing the dissipation (see Figs. S2 **b, f, and j**). This behavior is a consequence of the continuous quantum Zeno effect, as mentioned in the main text.

Time evolution of the squared norm in a quantum trajectory with a quantum jump

In Fig. S3, we plot time evolution of the squared norm $\langle \psi(\tau) | \psi(\tau) \rangle$ in the quantum trajectories shown in Fig. 4 in the main text. In the case of the Fermi-Hubbard model (Fig. S3**a**), the squared norm after the quantum jump is saturated at a finite value due to the existence of the dark state, which is the spin-symmetric ferromagnetic state [41]. The saturated value is determined by a squared overlap between the dark state and the state just after the quantum jump. Since the antiferromagnetic spin correlation in the initial state is washed out in the state after the quantum jump, the squared overlap, or the saturated value of the squared norm, takes a relatively larger value than that before the quantum jump. This property enables us to observe the ferromagnetic spin states with a reasonable probability.

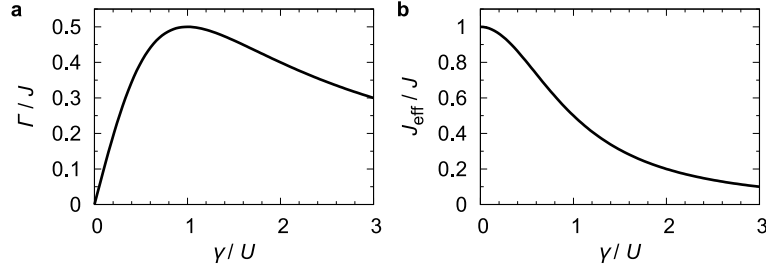


FIG. S1. **Dependence of the effective spin-exchange interaction on dissipation.** **a**, γ -dependence of the imaginary part of the effective spin-exchange interaction. **b**, γ -dependence of the real part of the effective spin-exchange interaction. Here J is given by $J = 4t^2/U$.

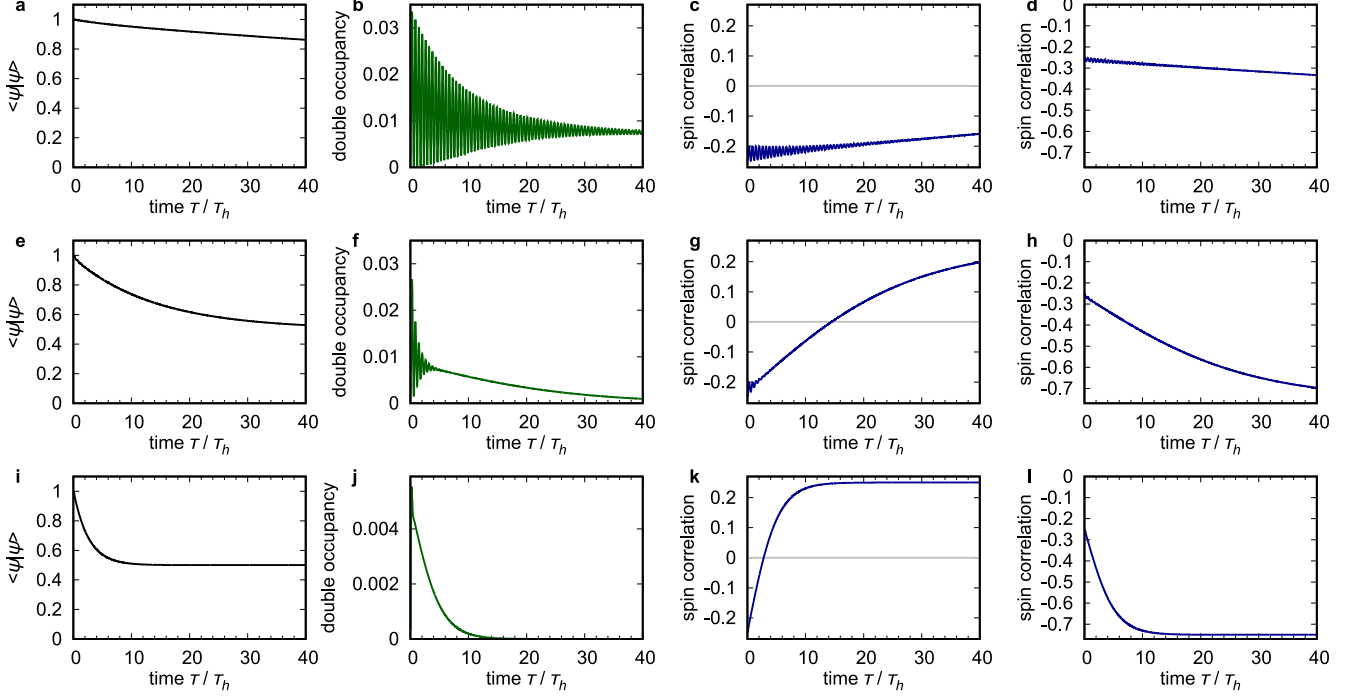


FIG. S2. **Dependence of the dynamics of the two-site dissipative Hubbard model on dissipation.** **a, e, i**, Time evolution of the squared norm $\langle \psi(\tau) | \psi(\tau) \rangle$. **b, f, j**, Time evolution of the double occupancy $\langle \psi(\tau) | \frac{1}{2}(n_{1\uparrow}^{(a)} n_{1\downarrow}^{(a)} + n_{2\uparrow}^{(a)} n_{2\downarrow}^{(a)}) | \psi(\tau) \rangle / \langle \psi(\tau) | \psi(\tau) \rangle$ ($a = f$ or b). The squared norm and the double occupancy take the same values for the Fermi and Bose Hubbard systems. **c, g, k**, Time evolution of the spin correlation $\langle \psi(\tau) | \mathbf{S}_1 \cdot \mathbf{S}_2 | \psi(\tau) \rangle / \langle \psi(\tau) | \psi(\tau) \rangle$ of the non-Hermitian Fermi-Hubbard model. **d, h, l**, Time evolution of the spin correlation of the non-Hermitian Bose-Hubbard model. The strength of the interaction is set to $U/t = 10$ in all figures, and the strength of dissipation is set to $\gamma/t = 0.1$ in **a-d**, $\gamma/t = 1$ in **e-h**, and $\gamma/t = 10$ in **i-l**. The unit of time is the inverse of the hopping rate $\tau_h = 1/t$.

On the other hand, in the case of the Bose-Hubbard model (Fig. S3b), the squared norm is not saturated at a finite value due to the absence of a dark state.

Time evolution with multiple quantum jumps

Figure S4 shows dynamics of the squared norm, the conditional correlator, and the standard correlator in a quantum trajectory with two jump events. Here the dissipative Fermi-Hubbard model with 8 sites is studied. The initial state is chosen to be the Néel state as in the main text. The first quantum-jump event at $\tau/\tau_h \simeq 3$ occurs at site $j = 0$ and decreases the particle number from eight to six. Subsequently, the second two-body loss event takes place at site $j = 4$ at time $\tau/\tau_h \simeq 4.7$, leaving four atoms in the system. As shown in Fig. S4b, the spin correlators involving sites at which the loss events take place are considerably affected by the quantum jumps (see $j = 0$ and $j = 3$ lines).

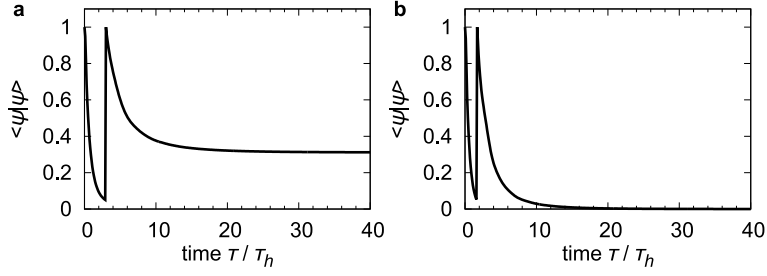


FIG. S3. **Squared norm in a quantum trajectory with a jump event.** Time evolution of the squared norm $\langle \psi(\tau) | \psi(\tau) \rangle$ in a quantum trajectory of the dissipative Fermi (a) and Bose (b) Hubbard model in which a loss event occurs at $\tau/\tau_h \simeq 3$ (a) and $\tau/\tau_h \simeq 1.7$ (b), respectively (here $\tau_h = 1/t$). The parameters and the initial states are the same as those in Fig. 4 in the main text.

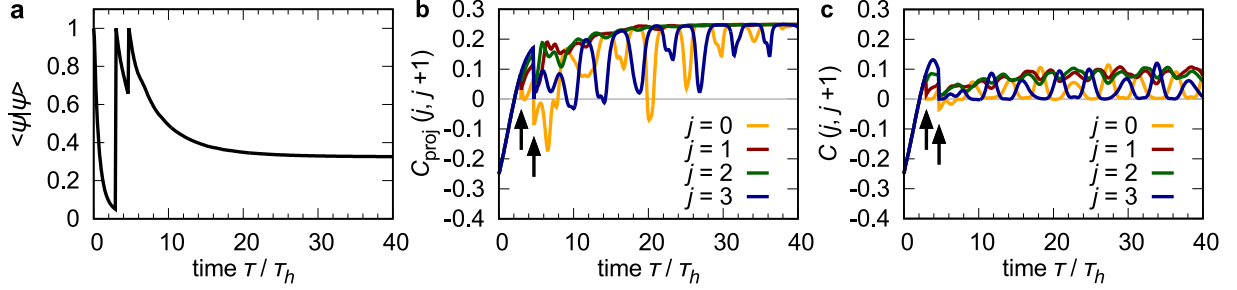


FIG. S4. **Dynamics in a quantum trajectory with multiple jump events.** Time evolution of the squared norm $\langle \psi(\tau) | \psi(\tau) \rangle$ (a), the conditional spin correlation $C_{\text{proj}}(j, j+1)$ (b), and the standard spin correlation $C(j, j+1)$ (c) in a quantum trajectory of the dissipative Fermi-Hubbard model. The parameters are set to $U/t = 10$ and $\gamma/t = 10$. The arrows indicate the times at which the quantum-jump events occur. The unit of time is the inverse of the hopping rate $\tau_h = 1/t$.

Remarkably, however, the other spin correlators are not quite disturbed (see $j = 1$ and $j = 2$ lines) and saturated at the completely ferromagnetic value $C_{\text{proj}}(j, j+1) = 0.25$ in a time scale comparable with that in the quantum trajectory without loss events shown in Fig. 3b. Such a feature is not clearly observed in the standard correlators (Fig. S4c) and can thus be first detected by using the conditional correlators which are enabled by quantum-gas microscopy.